Front. Earth Sci. 2015, 9(4): 722–731
DOI 10.1007/s11707-015-0538-z

RESEARCH ARTICLE

Merging daily sea surface temperature data from multiple satellites using a Bayesian maximum entropy method

Shaolei TANG[1,2], Xiaofeng YANG (✉)[1], Di DONG[1,2], Ziwei LI[1]

1 State Key Laboratory of Remote Sensing Science, Institute of Remote Sensing and Digital Earth, Chinese Academy of Sciences, Beijing 100101, China
2 University of Chinese Academy of Sciences, Beijing 100049, China

Abstract Sea surface temperature (SST) is an important variable for understanding interactions between the ocean and the atmosphere. SST fusion is crucial for acquiring SST products of high spatial resolution and coverage. This study introduces a Bayesian maximum entropy (BME) method for blending daily SSTs from multiple satellite sensors. A new spatiotemporal covariance model of an SST field is built to integrate not only single-day SSTs but also time-adjacent SSTs. In addition, AVHRR 30-year SST climatology data are introduced as soft data at the estimation points to improve the accuracy of blended results within the BME framework. The merged SSTs, with a spatial resolution of 4 km and a temporal resolution of 24 hours, are produced in the Western Pacific Ocean region to demonstrate and evaluate the proposed methodology. Comparisons with *in situ* drifting buoy observations show that the merged SSTs are accurate and the bias and root-mean-square errors for the comparison are 0.15°C and 0.72°C, respectively.

Keywords sea surface temperature (SST), Bayesian maximum entropy (BME), remote sensing, data fusion

1 Introduction

Sea surface temperature (SST) is an important geophysical parameter for various applications such as monitoring climate change (Smith and Reynolds, 2003) and reconstructing meso-scale and small-scale dynamics (Li et al., 2001a; Isern-Fontanet et al., 2006; Chao et al., 2009; Tandeo et al., 2014). In addition, SST is also a key input parameter for oceanic and atmospheric models such as the Ocean General Circulation Model (Yamamoto and Hirose, 2007). Satellite observation is a major source for obtaining the global distribution of SST, which can be derived from either microwave (MW) or infrared (IR) radiometer observations (Li et al., 2001b; Zhou et al., 2012). However, the SST data produced from IR and MW sensors have different characteristics and accuracies. IR SSTs have considerably high spatial resolutions (normally approximately 1 km). However, they are vulnerable to various atmospheric contaminants such as cloud cover and high concentrations of aerosols (Guan and Kawamura, 2003), resulting in spatial discontinuity and significant missing data rates. In contrast, MW SSTs are comparatively resistant to clouds and aerosols, thus offering high spatial coverage. However, MW SSTs have lower resolutions (approximately 25 km), and cannot be retrieved in coastal regions.

In view of the highly complementary characteristics of IR and MW SST products, several SST fusion methods have been proposed (Kawamura, 2004; Alvera-Azcárate et al., 2005; Reynolds et al., 2005; Sakaida et al., 2005; Kawai et al., 2006; Wang and Xie, 2007; Chao et al., 2009; Donlon et al., 2012; Li et al., 2013b). Among them, the Objective Analysis (OA), Optimum Interpolation (OI) and VARiational (VAR) methods are the most commonly used algorithms for blending SSTs. In addition, there are alternative SST fusion methods such as Bayesian Maximum Entropy (BME) and Data INterpolating Empirical Orthogonal Functions (DINEOF). The OI method can smooth the fine characteristics of SST products in space, thus limiting its application near the coast (Li et al., 2013b). In addition, it is necessary for *a priori* information about the error statistics of input data, which is often poorly known (Bennett, 2002). The VAR algorithm applies the same mathematical principle used by OI (Lorenc, 1986) but uses different numerical implementation. Like OI, one disadvantage of the VAR algorithm is the background error

Received April 5, 2015; accepted June 8, 2015

E-mail: yangxf@radi.ac.cn

variances and the observational error covariances are difficult to ascertain and somewhat subjectively specified (Li et al., 2013b). DINEOF merely employs a single data source and cannot acquire accurate high-resolution merged SSTs in equatorial regions because of year-round cloudiness. The BME method is a modern spatiotemporal geostatistical technique based on a sophisticated mathematical theory of space-time interpolation. BME has been successfully applied to merge remotely sensed data such as Ozone (Christakos et al, 2004), Leaf Area Index (LAI) (Li et al, 2013a) and SST (Li et al, 2013b). It can integrate less precise and uncertain "soft" data and express them as probability distributions or uniform distributions. There are two major advantages to this feature: first, we can integrate not only exact measurements ("hard data") but also soft data with uncertainty explicitly expressed, which greatly contributes to accurately predicted results. Second, when blending data of different spatial observation scales, an error model linking data of different spatial resolutions can convert data of coarse resolution to corresponding soft data of fine resolution, which can then be integrated in the BME framework. As a result, the scale issue due to discrepancies in spatial resolutions is solved and the uncertainty caused by the scale issue is effectively taken into account (Lee et al., 2008). The successful application of the BME method in producing 8-day average SSTs provides a certain confidence in extending the BME method to produce daily SST products. Compared with 8-day IR SSTs, daily IR SSTs have considerably lower spatial coverage. To overcome this drawback, the BME method used in Li et al. (2013b) must be optimized to produce daily SST blending data. The primary goal of this study is to produce spatially complete, accurate daily SST products by merging various satellite SSTs using the BME fusion method. To achieve this goal, a new spatiotemporal covariance model of the SST field is introduced and time-adjacent SST information is imported to improve the spatial coverage. In addition, AVHRR 30-year SST climatology data are also added as new background *a priori* knowledge to improve the fusion accuracy. The study area and data used in this study are introduced in Section 2. In Section 3, the proposed methodology is briefly presented. Section 4 shows the merging experiments and validation results. Finally, discussion and conclusions are presented in Section 5.

2 Study area and data description

2.1 Study area

The study area is part of the west-central Pacific Ocean (see Fig. 1). The air-sea interactions over the west-central Pacific Ocean have a remarkable impact on the short-term climate variations over China; when the SST of Western Pacific Ocean in winter is unusually warmer than normal, the result is drought in northern China and floods in southern China. Colder SSTs tend to do the opposite, so it is important to improve the accuracy and spatial resolution of SST products in the west-central Pacific Ocean area. To assure computing efficiency, we split the entire study area into six sub-regions of equal size.

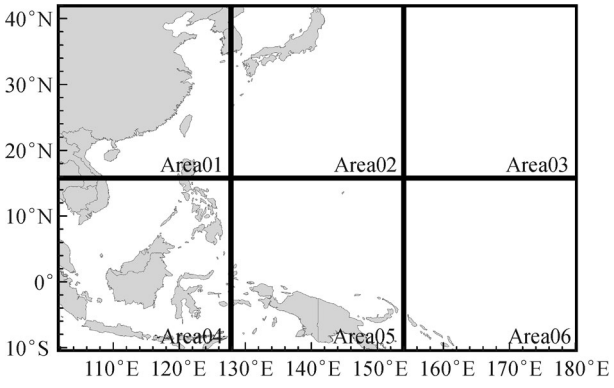

Fig. 1 The study area of this study (10°S – 40°N, 100°E – 180° E).

2.2 Data

2.2.1 Satellite data

MODIS SSTs, AVHRR SSTs, AMSR-E SSTs, TMI SSTs, and AVHRR climatology data in 2006 are used in this study. The MODIS SSTs are provided by the Ocean Color website (available online at http://oceancolor.gsfc.nasa.gov/, Brown et al., 1999). The AVHRR SSTs and climatology data are obtained from the US National Oceanographic Data Center and GHRSST (available online at http://pathfinder.nodc.noaa.gov, Casey et al., 2010), and the time span of the climatology data is from 1982 through 2008. The AMSR-E SST (Wentz and Meissner, 2000) and TMI SST (Gentemann et al., 2004) data are both produced and provided by Remote Sensing Systems (available online at http://www.remss.com/). The specifications of these satellite SSTs are shown in Table 1.

The data are typically provided with quality flags, so we select those SSTs with the most restrictive flags. To eliminate outliers, we calculate the standard deviation (SD) for each SST and remove any SSTs that are more than 3 SDs from the mean. To optimally utilize daytime retrievals, two continuous steps are performed. First, we use the simple empirical model of diurnal warming developed by Gentemann et al. (2003) to remove the warming of AVHRR and TMI retrievals. Second, we adjust the MODIS and AMSR-E daytime data through regression against the revised AVHRR and TMI retrievals, respectively.

Table 1 Specifications of the satellite derived SST products used in this study.

SST data	Spatial range	Spatial resolution /km	Time range	Temporal resolution /hours
MODIS SST	100° E–180° E, 10° S–40° N	4	2006	12
AVHRR SST		4		12
AMSR-E SST		25		12
TMI SST		25		12
AVHRR climatology data		4		24

2.2.2 *In situ* data

The *in situ* data used in our study are the drifting buoy SST measurements collected and processed by the Atlantic Oceanographic and Meteorological Laboratory (http://www.meds-sdmm.dfo-mpo.gc.ca). These are measurements obtained at a depth of 0.3 m during four daily observations at 0:00, 6:00, 12:00, and 18:00 UTC. To minimize the possible diurnal warming of *in situ* SSTs, we select the minimum value of the four observations as the daily *in situ* SST. The *in situ* SSTs of the same day belonging to the same grid square are then averaged.

2.2.3 MW_IR OI SST

The operational Optimally Interpolated (OI) SST daily products used for comparison with the merged SSTs are provided by remote sensing systems (http://www.remss.com/measurements/sea-surface-temperature/oisst-description). These products are blended together using the OI scheme described in Reynolds and Smith (1994) with microwave and IR data. The SSTs are frequently referred to as MW_IR OI SST and their spatial resolutions are 9 km.

3 Methodology

3.1 The BME method

As one of the modern spatiotemporal geostatistics techniques, BME does not make any of the restrictive assumptions of conventional interpolation techniques (Christakos et al., 2004). In the BME context, the SST data are continuous at pixel scale. Under the hypothesis that various adjacent SST observations are available, the nonlinear mean estimation $\hat{x}_{k,\mathrm{mean}}$ of SST at the estimation point (x, y) at time t can be calculated from Eq. (1):

$$\hat{x}_{k,\mathrm{mean}} = \int \mathrm{d}x_k x_k f^*(x_k|x_{\mathrm{Soft}},x_{\mathrm{Hard}}), \tag{1}$$

where $f^*(x_k|x_{\mathrm{Soft}},x_{\mathrm{Hard}})$ is the posterior probability density function (PDF) that is consistent with the adjacent SST observations available. x_{Soft} and x_{Hard} denote the soft and hard values of the adjacent grids, respectively. The soft data are measurements with errors that cannot be ignored and are always described in the form of probability functions or intervals of values, whereas the hard data are exact measurements with negligible errors.

The posterior PDF at the estimation point is updated from the prior PDF through the application of the operational Bayesian conditionalization rule when hard and soft data are involved. The prior PDF is obtained by maximizing the entropy under the constraint of general knowledge bases of the SST field. General knowledge bases typically include space-time statistics (such as multiple-point, nonlinear, and high-order statistics), physical laws, primitive equations, and governing relationships; this study utilizes the mean and covariance moment of the SST field. The BME's action principle of choice is the expected information maximization in light of the general knowledge bases. To maximize the expected information, we essentially maximize the corresponding entropy function. With the general knowledge and maximum entropy theory, we can obtain the exact form of the general knowledge-based PDF.

3.2 Error model linking different spatial scales data

This study utilizes the approach described by Lee et al. (2008) to account for the error caused by different spatial scales.

$X(s)$ and $Z(s')$ are both spatial random fields (SRFs). $X(s)$ is a local-scale SRF representing the spatial distribution of the variable X centered at s, and $Z(s')$ is defined as the average of $X(s)$ over a 2-D spatial domain A centered at s'.

$$Z(s') = \int_{\mu \in A_{s'}} \mathrm{d}\mu X(\mu)/\|A_{s'}\|. \tag{2}$$

To analyze the relationship between the local scale $X(s)$ and the A-scale $Z(s')$, a new spatial random field $Y_{(s,s')}$ is defined:

$$Y_{(s,s')} = X(s) - Z(s'). \tag{3}$$

When the spatial random field is homogeneous and the mean trend is removed, the expected value of $Y_{(s,s')}$, i.e., $E(Y_{(s,s')})$ is zero.

The variance describing the uncertainty associated with the observation scales can be written as

$$\sigma_Y^2 = \sigma_X^2 - 2\left\|A_{s'}\right\|^{-1}\int_{\mu\in A_{s'}} \mathrm{d}\mu C_X(|s'-\mu|) + \left\|A_{s'}\right\|^{-2}\int_{\mu\in A_{s'}}\mathrm{d}\mu\int_{\mu'\in A_{s'}}\mathrm{d}\mu' C_X(|\mu-\mu'|), \quad (4)$$

where σ_X^2 is the variance of the SRF $X(s)$ and C_X is the covariance between $X(s')$ and $X(s)$. Therefore, we can obtain a probabilistic soft datum χ_s for the local scale X at point s given a A-scale observed value ζ at point s':

$$f_s(\chi_s|\zeta) = \phi\left(\chi_s; E(Y_{(s,s')}) + \zeta, \sigma_Y^2\right) \Rightarrow N\left(E(Y_{(s,s')}) + \zeta, \sigma_Y^2\right). \quad (5)$$

Because IR SSTs have a higher resolution and can reflect the details of SST spatial features, we regard them as hard data. MW SSTs are transformed to corresponding soft data with a Gaussian probability distribution using the error model described above. In addition, we introduce AVHRR climatology data into our method to acquire soft data at estimation points, and these soft data are also expressed in the form of a Gaussian probability distribution. The means are the exact values of the climatology data and the SDs are equal to 3 SDs of climatology data. The primary goal of using AVHRR climatology data is to define the preliminary pattern of the SST field in the estimation regions and improve the accuracy of the merged SSTs.

3.3 Trend analysis

According to the BME method, the spatial estimation process operates on de-trended data. It is essential to quantify and remove large-scale effects prior to investigating the autocorrelation structure of the data (Spadavecchia and Williams, 2009). Therefore, we must conduct an SST field trend analysis and remove the trend before modeling the covariance function.

The SST distribution is represented by the spatiotemporal random field

$$\mathrm{SST}(s,t) = \overline{\mathrm{SST}}(s,t) + \mathrm{SST}_{\mathrm{ano}}(s,t), \quad (6)$$

where s represents space and t represents time. $\overline{\mathrm{SST}}(s,t)$ is the space-time mean trend of the SST, and it can be calculated from the BMElib package (Yu et al., 2007) by using a moving window average of $\mathrm{SST}(s,t)$ data with an exponential space/time filter. The residual field $\mathrm{SST}_{\mathrm{ano}}(s,t)$ is homogenous in space and stationary in time.

3.4 Space/time covariance model

The covariance function describes variability in space and time, and its value will typically decrease as distance (space or time) increases (Cressie, 1992). This study uses a composite space/time covariance model with nested exponential and Gaussian components as shown in Eq. (7). We select the following space/time model rather than a space model because the former can integrate time adjacent SSTs and produce more accurate and informative predictions (Christakos and Serre, 2000; Christakos et al, 2001):

$$c_X(r_{ij},\tau_{ij}) = c_1 \mathrm{e}^{\frac{-3r_{ij}}{a_{r1}}}\mathrm{e}^{\frac{-3\tau_{ij}}{a_{\tau 1}}} + c_2 \mathrm{e}^{\frac{-3r_{ij}^2}{a_{r2}^2}}\mathrm{e}^{\frac{-3\tau_{ij}^2}{a_{\tau 2}^2}}, \quad (7)$$

where $r_{ij} = |s_i| - |s_j|$ is the spatial distance between any pair of locations and $\tau_{ij} = |t_i| - |t_j|$ is the corresponding temporal distance. c_1 and c_2 denote the sill coefficients, a_{r1} and a_{r2} denote the spatial ranges of the fluctuation, and $a_{\tau 1}$ and $a_{\tau 2}$ denote the temporal ranges of the fluctuation. The experimental space/time covariance of the SST residual is calculated for pairs of points $\mathrm{SST}_{\mathrm{ano}}(i)$ and $\mathrm{SST}_{\mathrm{ano}}(j)$ at spatial and temporal lags r_{ij} and τ_{ij}, respectively. A theoretical model for the SST covariance can then be obtained by fitting the non-separable space/time function described above to the experimental covariance.

The processing flow diagram of this study is shown in Fig. 2.

4 Experimental results

Using the satellite data described above during the one-year period of 2006, 4-km daily cloud-free SST products are generated in the Asia-Pacific region of 10°S –40°N, 100°E–180°E.

4.1 Modeling space/time correlation structure of SST field

The parameters of the covariance model in Eq. (7) fitted to the experimental residual SSTs are shown in Table 2, and the corresponding model is plotted in Fig. 3. The variabilities of SSTs in sub-regions Area01 and Area04 have greater covariance values than the other sub-regions, and the variability of SSTs in sub-region Area06 has the lowest covariance value. This may be because sub-regions Area01 and Area04 are closer to land and their SSTs are thus easily affected by the continental climate and overland flow. In addition, the variabilities of small-range SSTs in the nearshore areas (Area01 and Area04) are greater than those of large-range SSTs, whereas the opposite characteristics are revealed in the pelagic regions (Area03 and Area06).

4.2 Validation of merged SSTs using drifting buoy measurements

The comparison of the blended SSTs with *in situ* measurements is plotted in Fig. 4(a); the total number of *in situ* data points is 50,726. The bias and the root-mean-square error (RMSE) are 0.15°C and 0.72°C, respectively. We then use the BME method employed in Li et al. (2013b) to produce blended SST products (hereafter called 'pre-improved SSTs'), and their comparison results are

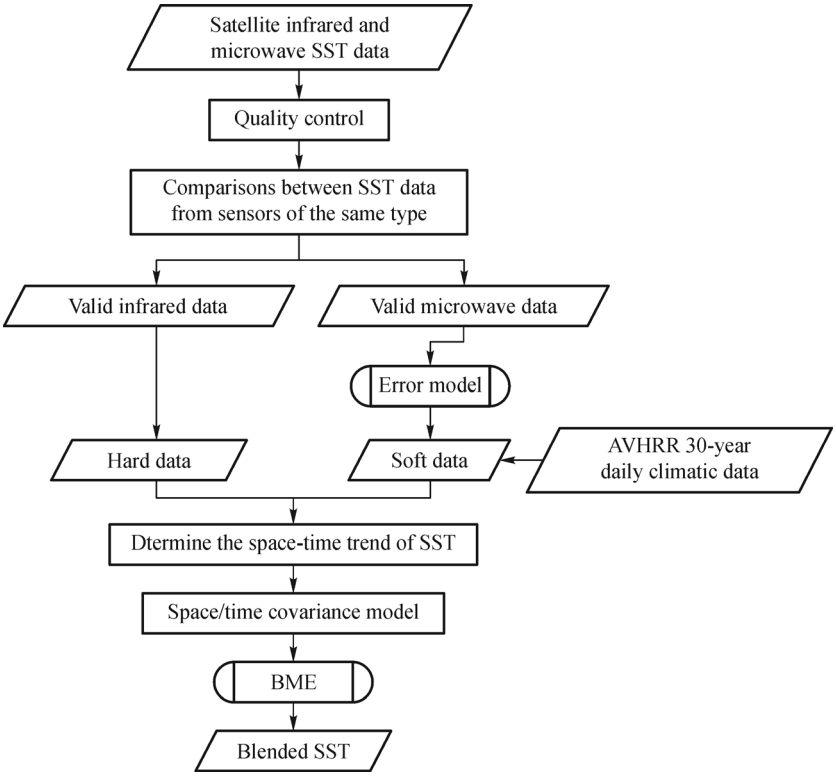

Fig. 2 Flowchart of the BME blending method proposed in this study.

plotted in Fig. 4(b). The total number of corresponding *in situ* points is 45,367 because of the relatively low spatial coverage of the pre-improved SST products (the daily average availabilities of pre-improved products is 90.7% compared with the full spatial coverage of the blended SSTs using the proposed method). The bias of the pre-improved SSTs is 0.18°C, with an RMSE 0.83°C. In general, the proposed method provides better results in terms of accuracy and spatial coverage compared with the one used in Li et al. (2013b).

To demonstrate that adding AVHRR climatology data can improve SST mapping accuracy, we recalculate the interpolation using the same satellite SSTs without the AVHRR climatology data. The comparison between the interpolation results and the *in situ* data is plotted in Fig. 4(c). As seen in Fig. 4(c) and Fig. 4(a), the prediction results without AVHRR climatology data are less accurate in terms of both bias and RMSE.

We also make a comparison between the *in situ* buoy observations and the microwave plus infrared (MW_IR) OI SST products provided by Remote Sensing Systems. We can see in Fig. 4(d) that the bias and RMSE of the operational MW_IR SSTs are slightly lower than the proposed method. However, the resolution of the MW_IR SSTs is 9 km, which is much coarser than the proposed method (4 km). These comparison results show that this new method not only enhances the spatial resolution of the SST products but also maintains their accuracies.

Overall, the BME method proposed in this study can improve merging accuracy by incorporating the AVHRR climatology data and making the most of the soft data transformed by the MW data along with the AVHRR climatology data.

Because the SST patterns in these regions vary in different times, we compare the merged results with the drifting buoy data in four time frames and plot the distribution of the corresponding buoy data and these biases to assess the accuracy of the merged SSTs in more detail. The compared results are shown in Fig. 5. The bias and RMSE of the merged SSTs in JFM (Jan-Feb-Mar) as a whole are relatively greater than those in the other three time frames. The biases and RMSEs in AMJ (Apr-May-Jun), JAS (Jul-Aug-Sep), and OND (Oct-Nov-Dec) are comparable. The preliminary reason for greater bias and RMSE in JFM is the lack of accurate IR SSTs; therefore, the soft data, including microwave and climatology SSTs, occupy a greater proportion in the fusion framework. In addition, the accuracy of merged SSTs in the tropical western Pacific is greater than those in other regions in all four time periods.

4.3 Spatial-temporal evolution of Kuroshio Current revealed by merged SSTs

In addition to the improvement of spatial coverage, another objective of merging SSTs is preserving the fine-scale

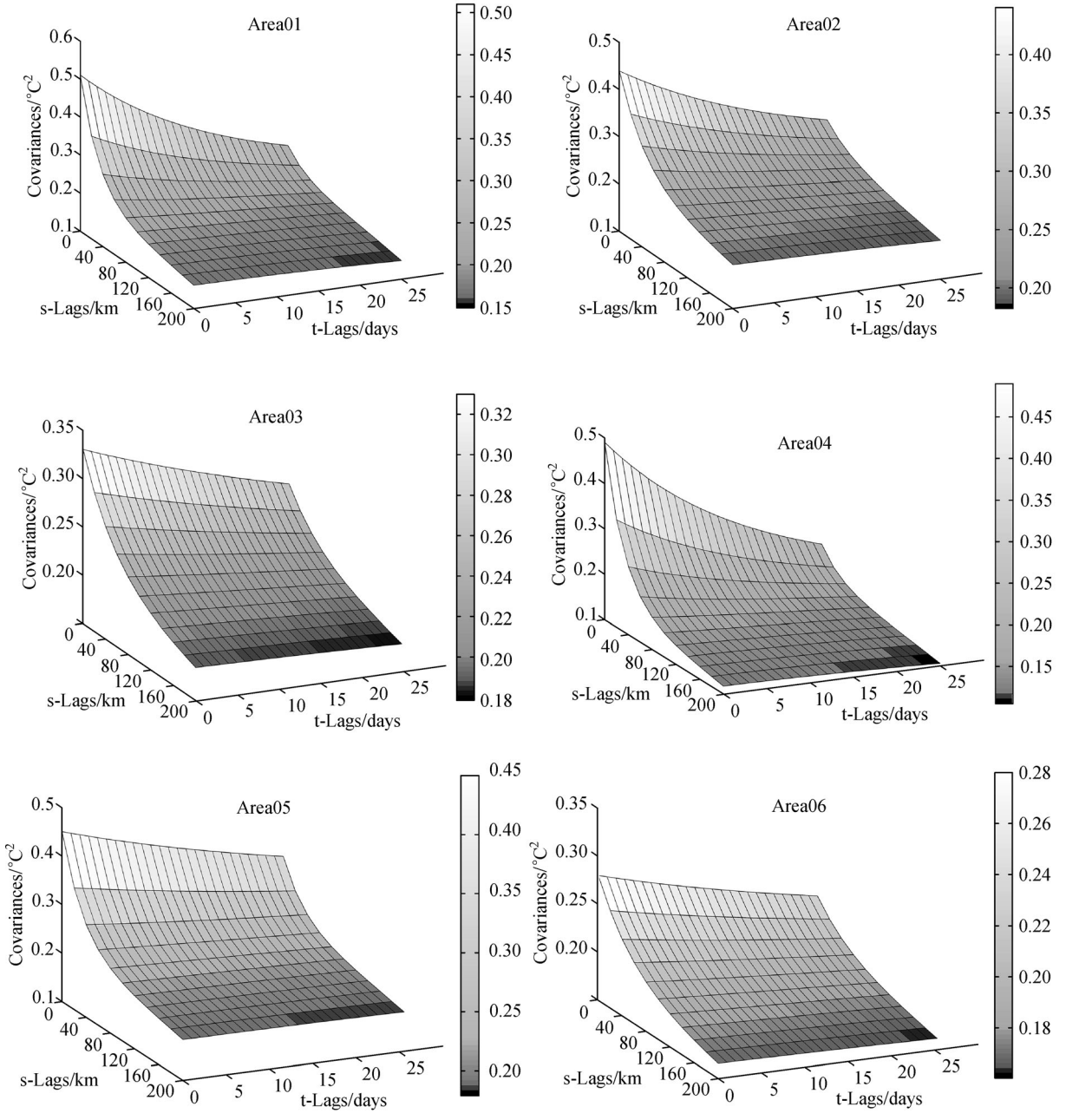

Fig. 3 The spatiotemporal covariance model of different sub-regions as a function of the spatial lag (s-Lag) and the temporal lag (t-Lag).

Table 2 Parameters of space–time covariance model of different sub-regions

Area	c_1/°C^2	c_2/°C^2	a_{r1}/km	a_{r2}/km	$a_{\tau 1}$/days	$a_{\tau 2}$/days
Area01	0.32	0.19	104	832	10	32
Area02	0.23	0.21	152	1040	13	45
Area03	0.14	0.19	200	1340	25	67
Area04	0.35	0.14	104	792	10	28
Area05	0.24	0.21	112	924	25	60
Area06	0.11	0.17	200	1400	25	72

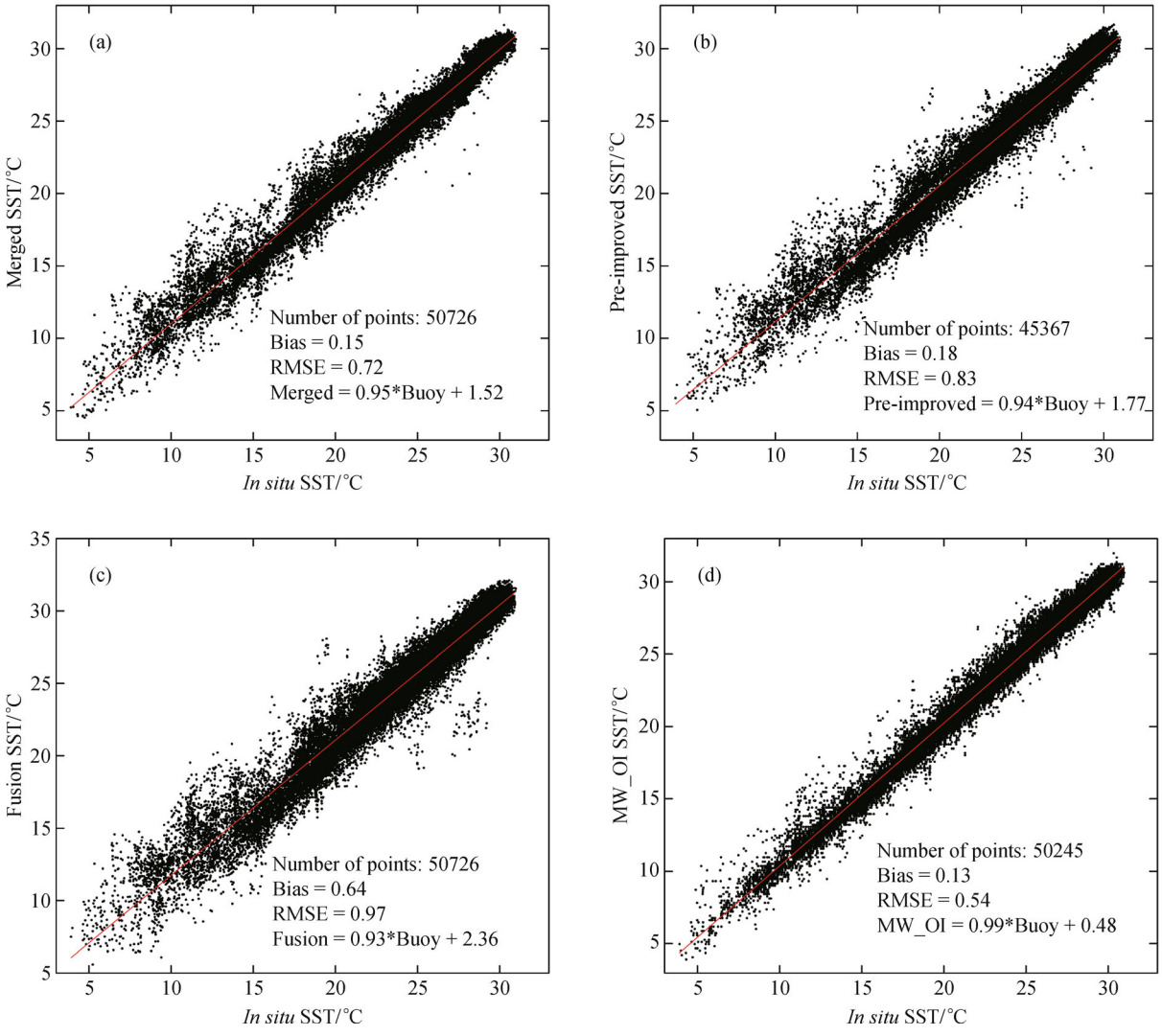

Fig. 4 Comparisons between *in situ* buoy observations and merged SSTs using different fusion methods: (a) the proposed BME method; (b) existing BME method; (c) the proposed BME method without using AVHRR climatology data; (d) operational MW_OI SST product.

spatial pattern of IR SST products, which can clearly reveal the small-scale spatial and temporal ocean structures associated with ocean currents and upwelling (Li et al., 2001c). To demonstrate the potential ability of merged SSTs in revealing the spatial-temporal evolution of small-scale structures, we plot a Hovmöller diagram (Fig. 7) of the PN section (Fig. 6) in the East China Sea. The PN section is the typical cross-section of the Kuroshio Current's principle axis in the East China Sea and has become one of the most important sections used to study the spatial-temporal evolution of the Kuroshio Current. Figure 7(a) shows the Hovmöller diagram plot using the merged SSTs and Fig. 7(b) provides a reference plot using the MW_ OI SST products. Clearly we can see the spatial-temporal evolution of SSTs in the PN section, and the characteristics shown by these two pictures are almost identical. In addition, we calculate the local variance of the merged SSTs and MW_OI products to evaluate these abilities of showing the fine-scale spatial pattern. A greater local variance reveals a finer spatial pattern. The local variance of merged SSTs is computed within a 25×25 moving window and the local variance of the MW_OI product is computed within a 9×9 moving window that covers nearly the same area as the former one. The result is shown in Fig. 8, and we can see that the local variance of the merged SSTs is a bit greater than that of the MW_OI SSTs, which means that the merged SSTs can capture finer spatial patterns.

5 Discussion and conclusions

This study employed a BME method to produce SST products with a spatial resolution of 4 km and a temporal resolution of 24 hours. Within the framework of the BME, we constructed a space/time covariance model of an SST

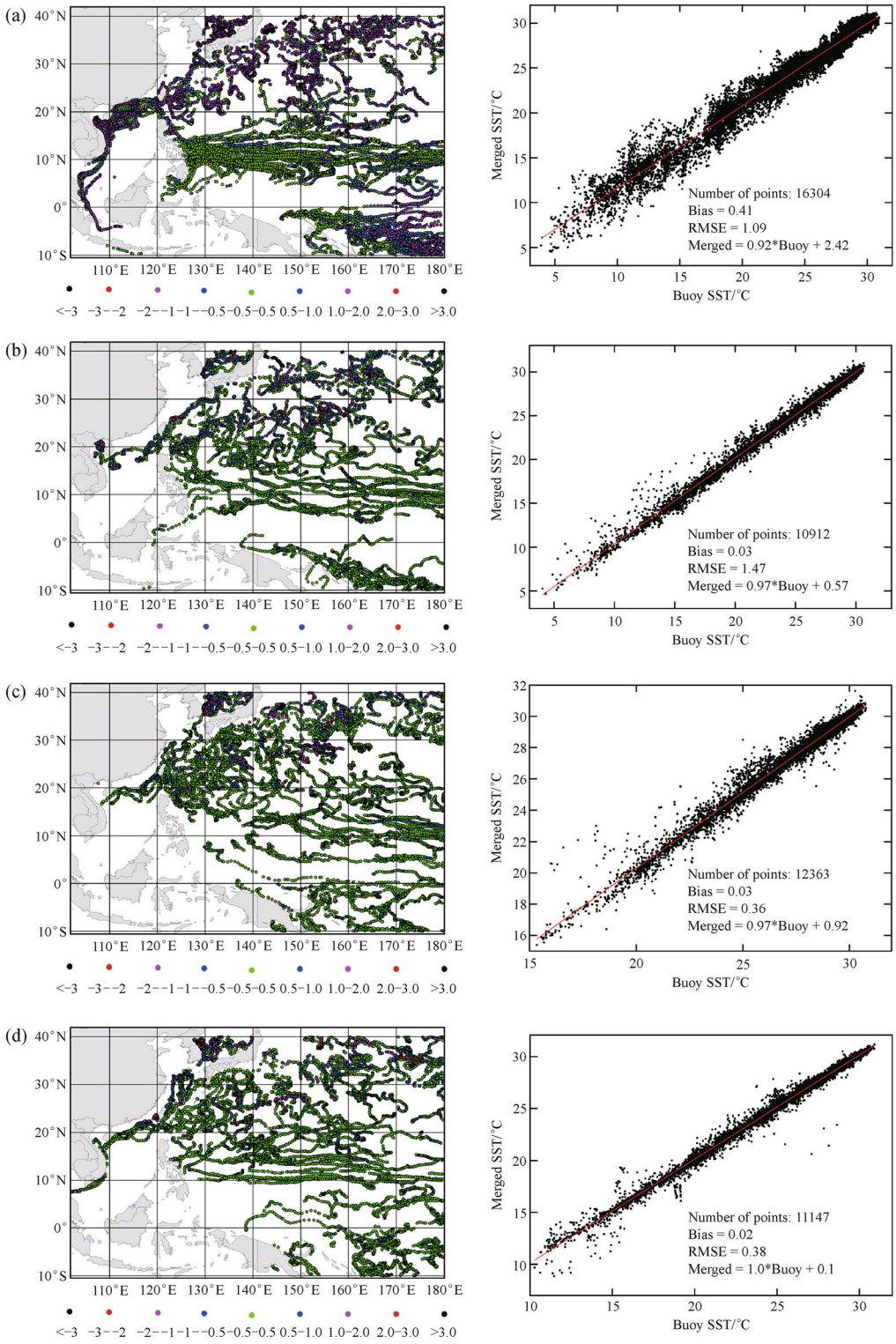

Fig. 5 Comparisons between merged SSTs and *in situ* buoy observations and the corresponding spatial distribution of the data in (a) JFM, (b) AMJ, (c) JAS, and (d) OND.

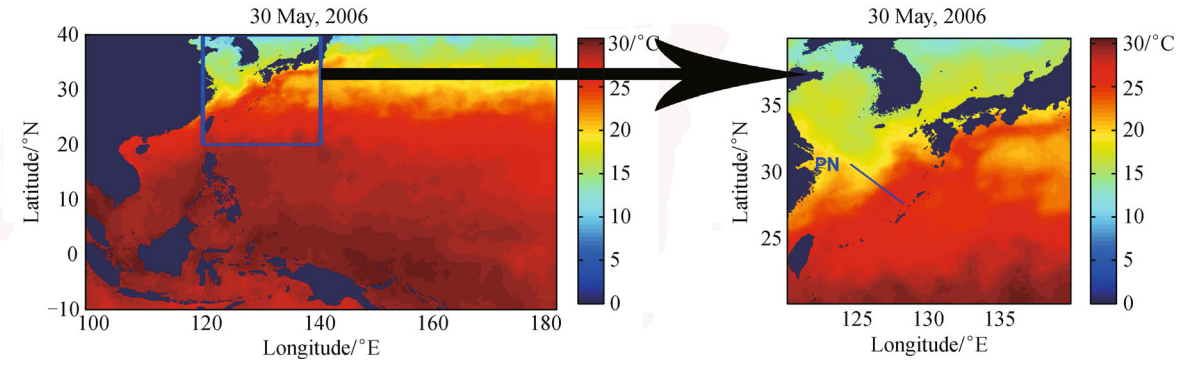

Fig. 6 Merged SST on 30 May, 2006. (a) SST distribution over the study area; the area in the blue box is where the Kuroshio Current flows. (b) The amplified area of blue box in the left picture; the blue line is the PN section in the East China Sea.

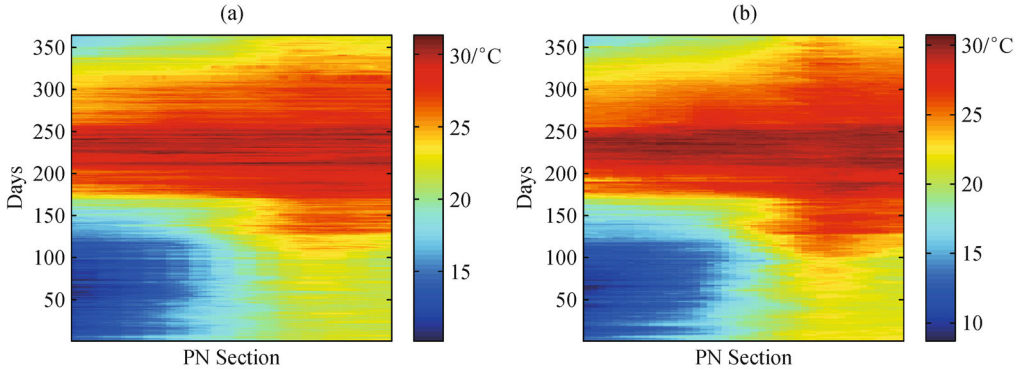

Fig. 7 The Hovmöller diagram of SSTs in 2006 in the PN section calculated by (a) merged SSTs and (b) MW_OI SST product.

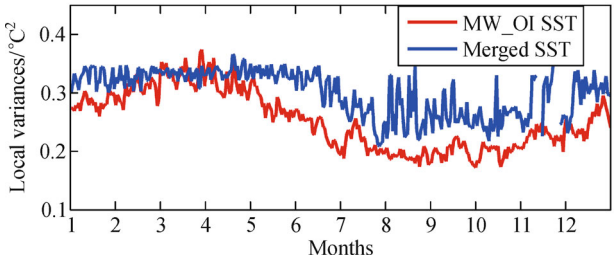

Fig. 8 The local variances calculated by merged SSTs and MW_OI SST product.

field rather than a space covariance model to integrate more SSTs. We also introduced AVHRR 30-year climatology data as soft data in the estimation points. The results showed good performance in acquiring merged SSTs with high accuracy and spatial coverage. An evaluation using drifting buoy SST observations showed a bias of 0.15°C and an RMSE of 0.72°C. Furthermore, the accuracy of the merged SSTs was evaluated in different times and showed that the bias and RMSE in JFM was a bit greater than those in the other three time frames. To evaluate the merged SSTs' ability to capture fine spatial patterns, a Hovmöller diagram of SSTs in the PN section of the East China Sea was plotted, and the local covariances of the merged SSTs and MW_OI SST products were compared and showed good results. We did not attempt to make any prior assumptions and objectively specified the parameters, except for the determination of the space/time covariance model because the model fitting approach was based on visual inspection. In addition, we did not include *in situ* SSTs, even though they were highly accurate, because it is difficult to eliminate the error caused by different spatial scales of *in situ* observations and satellite SSTs. If this issue can be resolved, the accuracy of merged SSTs may be further improved.

Acknowledgements This study was supported by the National Natural Science Foundation of China (Grant Nos. 41201350 and 41371355). We sincerely thank the University of North Carolina Bayesian Maximum Entropy (UNC-BME) laboratory at the UNC at Chapel Hill for supplying the BME codes.

References

Alvera-Azcárate A, Barth A, Rixen M, Beckers J M (2005). Reconstruction of incomplete oceanographic data sets using

empirical orthogonal functions: application to the adriatic sea surface temperature. Ocean Model, 9(4): 325–346

Bennett A F (2002). Inverse Modeling of the Ocean and Atmosphere. London: Cambridge University Press

Brown O B, Minnett P J, Evans R, Kearns E, Kilpatrick K, Kumar A, Sikorski R, Závody A (1999). MODIS Infrared Sea Surface Temperature Algorithm- Algorithm Theoretical Basis Document (Version 2.0). University of Miami

Casey K S, Brandon T B, Cornillon P, Evans R (2010). Oceanography from Space. Springer Netherlands, 273–287

Chao Y, Li Z, Farrara J D, Hung P (2009). Blending sea surface temperatures from multiple satellites and *in situ* observations for coastal oceans. J Atmos Ocean Technol, 26(7): 1415–1426

Christakos G, Kolovos A, Serre M L, Vukovich F (2004). Total ozone mapping by integrating databases from remote sensing instruments and empirical models. IEEE Trans Geosci Rem Sens, 42(5): 991–1008

Christakos G, Serre M L (2000). BME analysis of spatiotemporal particulate matter distributions in North Carolina. Atmos Environ, 34 (20): 3393–3406

Christakos G, Serre M L, Kovitz J L (2001). BME representation of particulate matter distributions in the state of California on the basis of uncertain measurements. Journal of Geophysical Research: Atmospheres (1984–2012), 106 (D9): 9717–9731

Cressie N (1992). Statistics for Spatial Data. Terra Nova, 4(5): 613–617

Donlon C J, Martin M, Stark J, Roberts-Jones J, Fiedler E, Wimmer W (2012). The operational sea surface temperature and sea ice analysis (Ostia) system. Remote Sens Environ, 116(2): 140–158

Gentemann C L, Donlon C J, Stuart-Menteth A, Wentz F J (2003). Diurnal signals in satellite sea surface temperature measurements. Geophys Res Lett, 30(3): 1140–1143

Gentemann C L, Wentz F J, Mears C A, Smith D K (2004). In situ validation of tropical rainfall measuring mission microwave sea surface temperatures. Journal of Geophysical Research: Oceans, 109 (C4): 249–260

Guan L, Kawamura H (2003). SST availabilities of satellite infrared and microwave measurements. J Oceanogr, 59(2): 201–209

Isern-Fontanet J, Chapron B, Lapeyre G, Klein P (2006). Potential use of microwave sea surface temperatures for the estimation of ocean currents. Geophys Res Lett, 33(24): L24608

Kawai Y, Kawamura H, Takahashi S, Hosoda K, Murakami H, Kachi M, Guan L (2006). Satellite-based high-resolution global optimum interpolation sea surface temperature data. Journal of Geophysical Research: Oceans (1978–2012), 111(C6): 285–293

Lee S L, Balling R, Gober P (2008). Bayesian maximum entropy mapping and the soft data problem in urban climate research. Ann Assoc Am Geogr, 98(2): 309–322

Li A, Bo Y, Chen L (2013a). Bayesian maximum entropy data fusion of field-observed leaf area index (LAI) and Landsat Enhanced Thematic Mapper Plus-derived LAI. Int J Remote Sens, 34(1): 227–246

Li A, Bo Y, Zhu Y, Guo P, Bi J, He Y (2013b). Blending multi-resolution satellite sea surface temperature (SST) products using Bayesian maximum entropy method. Remote Sens Environ, 135(4): 52–63

Li X, Pichel W, Clemente-Colon N P, Krasnopolsky V, Sapper J (2001a). Validation of coastal sea and lake surface temperature measurements derived from NOAA/AVHRR data. International Journal of Remote Sensing, 22(7): 1285–1303

Li X, Pichel W, Maturi E, Clemente-Colon P, Sapper J (2001b). Deriving the operational nonlinear multi-channel sea surface temperature algorithm coefficients for NOAA-15 AVHRR/3. International Journal of Remote Sensing, 22(4): 699–704

Li X, Zheng Q, Pichel W G, Yan X, Timothy Liu W, Clemente-Colon P (2001c). Analysis of coastal lee waves along the coast of Texas observed in advanced very high resolution radiometer Images. J Geophys Res, 106(C4): 7017–7025

Lorenc A C (1986). Analysis methods for numerical weather prediction. Q J R Meteorol Soc, 112(474): 1177–1194

Reynolds R W, Smith T M (1994). Improved global sea surface temperature analyses using optimum interpolation. J Clim, 7(6): 929–948

Reynolds R W, Zhang H, Smith T M, Gentemann C L, Wentz F (2005). Impacts of *in situ* and additional satellite data on the accuracy of a sea-surface temperature analysis for climate. Int J Climatol, 25(7): 857–864

Sakaida F, Takahashi S, Shimada T, Kawai Y, Kawamura H, Hosoda K, Guan L (2005). The production of the new generation sea surface temperature (NGSST-O ver. 1.0) in Tohoku University. Geoscience and Remote Sensing Symposium, 2005. IGARSS '05. IEEE, 2005: 2602–2605

Smith T M, Reynolds R W (2003). Extended reconstruction of global sea surface temperatures based on COADS data (1854–1997). J Clim, 16 (10): 1495–1510

Spadavecchia L, Williams M (2009). Can spatio-temporal geostatistical methods improve high resolution regionalisation of meteorological variables? Agric Meteorol, 149(6–7): 1105–1117

Tandeo P, Chapron B, Ba S, Autret E, Fablet R (2014). Segmentation of mesoscale ocean surface dynamics using satellite SST and SSH observations. IEEE Trans Geosci Rem Sens, 52(7): 4227–4235

Wang W, Xie P (2007). A multiplatform-merged (MPM) SST analysis. J Clim, 20(9): 1662–1679

Wentz F J, Meissner T (2000). AMSR Ocean Algorithm Theoretical Basis Document, Version 2. Remote Sensing Systems, Santa Rosa, CA

Yamamoto M, Hirose N (2007). Impact of SST reanalyzed using OGCM on weather simulation: a case of a developing cyclone in the Japan Sea area. Geophys Res Lett, 34(5): L05808

Yu H L, Kolovos A, Christakos G, Chen J, Warmerdam S, Dev B (2007). Interactive spatiotemporal modeling of health systems: the SEKS–GUI framework. Stochastic Environ Res Risk Assess, 21(5): 555–572

Zhou X, Yang X, Cheng L, Li Z (2012). Sensitivity analysis and validation of the single channel physical method for retrieving sea surface temperature. Journal of infrared and millimeter waves, 31(1): 91–96